

## Full Length Article

# CXCR4 mediates the effects of IGF-1R signaling in rodent bone homeostasis and fracture repair

Alessandra Esposito<sup>a</sup>, Michael Klüppel<sup>a</sup>, Brittany M. Wilson<sup>a</sup>, Sai R.K. Meka<sup>a</sup>, Anna Spagnoli<sup>a,b,\*</sup>

<sup>a</sup> Department of Orthopaedic Surgery, Rush University Medical Center, Chicago, IL, USA

<sup>b</sup> Department of Pediatrics, Rush University Medical Center, Chicago, IL, USA



## ARTICLE INFO

## Keywords:

CXCR4  
IGF-1R  
Fracture healing  
Endosteum  
Skeletal cells  
Non-union

## ABSTRACT

Non-union fractures have considerable clinical and economic burdens and yet the underlying pathogenesis remains largely undetermined. The fracture healing process involves cellular differentiation, callus formation and remodeling, and implies the recruitment and differentiation of mesenchymal stem cells that are not fully characterized. C-X-C chemokine receptor 4 (CXCR4) and Insulin-like growth factor 1 receptor (IGF-1R) are expressed in the fracture callus, but their interactions still remain elusive. We hypothesized that the regulation of CXCR4 by IGF-1R signaling is essential to maintain the bone homeostasis and to promote fracture repair. By using a combination of *in vivo* and *in vitro* approaches, we found that conditional ablation of IGF-1R in osteochondroprogenitors led to defects in bone formation and mineralization that associated with altered expression of CXCR4 by a discrete population of endosteal cells. These defects were corrected by AMD3100 (a CXCR4 antagonist). Furthermore, we found that the inducible ablation of IGF-1R in osteochondroprogenitors led to fracture healing failure, that associated with an altered expression of CXCR4. *In vivo* AMD3100 treatment improved fracture healing and normalized CXCR4 expression. Moreover, we determined that these effects were mediated through the IGF-1R/Insulin receptor substrate 1 (IRS-1) signaling pathway. Taken together, our studies identified a novel population of endosteal cells that is functionally regulated through the modulation of CXCR4 by IGF-1R signaling, and such control is essential in bone homeostasis and fracture healing. Knowledge gained from these studies has the potential to accelerate the development of novel therapeutic interventions by targeting CXCR4 signaling to treat non-unions.

## 1. Introduction

Regeneration is one of the most remarkable abilities of the skeleton. Fracture healing is a process emerging from a complex interaction of humoral, mechanical and biological factors. Impairment of one or more of these factors can result in failure of the bone to heal, a condition termed 'non-union'. [1] Non-unions are a significant health challenge affecting about 2 % of all bone fractures, and can be as high as 20 % for diaphyseal fractures. [2] The financial burden associated with a long healing process can often be extensive, affecting both patients and the healthcare systems. [3–6] A better understanding of the biology of fracture healing and the molecular risk factors and signaling pathways associated with non-union can lead to the development of novel therapeutic agents and implement treatment options to promote healing in patients that suffer from non-unions.

Mesenchymal stromal cells (MSC) are present in multiple tissues, including fat, bone marrow, endosteum and periosteum, umbilical cord and peripheral blood. [7] MSCs have the capacity to self-renew and to differentiate into osteoblasts, chondrocytes, adipocytes and connective tissue. [8] Their differentiation and lineages are determined by mechanical, chemical and hormonal stimuli, including cytokines and growth factors. [9–11] The ability to control the osteoblastic differentiation of MSCs has generated great interest for their potential use in non-union treatment. However, their nature and interactions with hormonal factors controlling their differentiation remain elusive. Compelling evidence, including from our own laboratory, have demonstrated that MSCs are recruited locally to the fracture site from the endosteum and periosteum and are the major functional contributors to the fracture callus. [12–14] Characterization of specific interplays between growth factors and MSCs can lead to identification of defective mechanisms

\* Corresponding author at: Department of Orthopaedic, 1725 West Harrison Street, Cohn Research Building, Room 502A, Chicago, IL 60612, USA.

E-mail address: [anna.spagnoli@rush.edu](mailto:anna.spagnoli@rush.edu) (A. Spagnoli).

underlying non-unions and to the establishment of novel therapeutic strategies for non-union healing.

C-X-C chemokine receptor 4 (CXCR4) is an alpha chemokine receptor specific for C-X-C motif-ligand-12 (CXCL12). CXCR4 and CXCL12 are expressed by perivascular reticular cells, endothelial cells, hematopoietic cells, MSCs and cells of the osteoblast lineage, [15] and they mediate numerous biological actions. In particular, in osteoblast lineage cells the CXCR4-CXCL12 axis has been reported to mediate cell homing [16] and differentiation. [17] Furthermore, CXCR4/CXCL12 axis has been reported to be expressed in the fracture callus, but its function has not been fully elucidated. [18,19]

Several growth factors and cytokines play orchestrated roles during the fracture healing process. [20–24] Specifically, the insulin-like growth factor 1 (IGF-1), has been shown to play critical roles in bone homeostasis, bone remodeling, and in regulating proliferation and differentiation of osteoprogenitor cells during fracture healing. [25–29] The effects of IGF-1 in bone homeostasis and regeneration have been shown to be mediated through endocrine, paracrine, and autocrine mechanisms. [30] In humans, an impairment of the growth hormone/IGF-1 axis has been reported to be involved in the biochemical mechanisms determining delayed or failed fracture healing. [28] Notably, low levels of circulating IGF-1 have been reported in patients with non-unions, [31,32] suggesting a potential role in the pathological mechanisms underlying failed or delayed fracture healing. Furthermore, it has been reported that IGF-1 plays a role in the consolidation of delayed union and high serum levels of IGF-1 correlated with successful treatment outcomes. [28,33–35] IGF-1 binding to IGF type 1 receptor (IGF-1R) triggers numerous intracellular signaling pathways, [36] including Insulin receptor substrate 1 (IRS-1). The relevance of IGF-1R signaling in fracture repair has been highlighted by studies in animal models carrying tissue specific deletions of IGF-1R [29,37–42] and IGF-1 [43–46] and by the evidence of IGF-1 treatment promoting fracture healing. [28,33–35] However, the mechanisms through which IGF-1 signaling regulates fracture repair are still not fully understood.

We hypothesized that the regulation of CXCR4 by IGF-1R signaling is essential to maintain the bone homeostasis and to promote fracture repair. To address this, we analyzed the effects of manipulating IGF-1R on CXCR4 by using a combination of *in vivo* and *in vitro* approaches.

## 2. Materials and methods

### 2.1. Antibodies and reagents

Primary antibodies and fluorochrome-conjugated secondary antibodies are summarized in Supplemental Table 1. Safranin O (S2255) was purchased from Fluka Chemical (Milwaukee, WI). Hematoxylin (H3136), Orange G (O7252), glacial acetic acid (A6283), aluminum ammonium sulfate (A2140), collagenase (C1889), cetylperidinium chloride (17776), trypsin (T6567) and 4OH-TAM (4-hydroxy-tamoxifen) (H6278) were obtained from Sigma Aldrich (St Louis, MO). Fast green (F7252) and sodium iodate (S4007) are from Fisher Scientific (Waltham, MA). The inhibitor AMD3100 (Plerixafor) was from AdooQ Bioscience (A13074, Irvine, California, USA).

### 2.2. Animal models

To generate Prx1-Cre<sup>+</sup>;Igf1R<sup>fl/fl</sup> heterozygous males mice, Igf1R<sup>fl/fl</sup> mice [82] (Jackson Laboratory, Bar Harbor, Maine, USA) were crossed with Prx1 limb enhancer driven-Cre transgenic males [83] (C57B/L6 background) (C. Tabin, Harvard Medical School), which drives Cre-expression in osteochondroprogenitors. Prx1-Cre<sup>+</sup>;Igf1R<sup>fl/fl</sup> mice were crossed with Igf1R<sup>fl/fl</sup> to produce Prx1-Cre<sup>+</sup>;Igf1R<sup>fl/fl</sup> (called IGF-1R<sup>CKO</sup>). We verified that IGF-1R expression was decreased (>80 %) in the tibia (after BM was flashed out) from IGF-1R<sup>CKO</sup> mice, compared to sex-matched controls (Suppl. Fig. 20A). Prx1CreER-GFP+/Igf1R<sup>fl/fl</sup> (called IGF-1R<sup>CKO</sup>) mutant mice were generated by crossing male Prx1-CreER-

GFP+/Igf1R<sup>fl/fl</sup> mice (Prx1-CreER-GFP is provided by Dr. Shunichi Murakami, Case Western Reserve University, Cleveland, Ohio, USA) [84] with female Igf1R<sup>fl/fl</sup> mice. The Irs1<sup>KO</sup> mice homozygous for Irs1 gene deletion were provided by Dr. C.R. Kahn. [85] We confirmed the genotypes of the transgenic mice by PCR analysis of genomic DNA isolated from mouse ears (Suppl. Fig. 20B). Genotyping was performed by PCR analysis using the primers reported in Supplemental Table 1. All mice had been backcrossed on the C57BL/6 strain for at least ten generations. All procedures used were consistent with the guidelines of the National Institutes of Health and approved by the Institutional Animal Care and Use Committees of Rush University Medical Center (Chicago, IL, USA).

### 2.3. Tibia fracture model

Semi-stabilized tibia fractures, in which intramedullary fixation enables relative stability to facilitate endochondral ossification, were produced in C57BL/6 background male mice between 8 and 10 weeks of age, as described. [86] The intramedullary pin was carefully removed after dissection. In male IGF-1R<sup>CKO</sup> mice, 4OH-TAM administrations were performed for 5 days (0.5 µg/g BW, from 2 days before to 2 days after fracture) (Fig. 3A). Mice were euthanized at PFD 0, 1, 7, 14 and 21. In studies where animals were injected with 4OH-TAM only male mice were used, because the concern of effects of 4OH-TAM on females that would potentially interfere with data interpretation. For treatment with AMD3100, IGF-1R<sup>CKO</sup> mice were intraperitoneally (*i.p.*)-injected with 2.5 mg/g BW of AMD3100-PBS solution twice per day on the 2 days preceding fracture and then twice daily from PFD 2 to PFD 7 post-fracture. Fractured bones were harvested at PFD 14 and 21 (Fig. 5A). IGF-1R<sup>CKO</sup> mice were subcutaneously (*s.c.*)-injected every other day with 2.5 mg/g BW of AMD3100-PBS solution per day from postnatal day 3 to postnatal day 28, at which point bones were harvested (Fig. 2E).

### 2.4. Micro-computed tomography analysis of unfractured tibias

Tibias and femurs from IGF-1R<sup>CKO</sup> (cKO) and control (Con) mice were used for micro-computed tomography (µCT) analysis (µCT 50; Scanco Medical AG, Bassersdorf, Switzerland). Briefly, right tibias and femurs were harvested from females and males of 4, 8 and 12 weeks-old IGF-1R<sup>CKO</sup> and control mice, fixed in 4 % paraformaldehyde in PBS overnight at 4 °C, rinsed, and scanned in 70 % ethanol. Scanned images were obtained at energy of level of 55 kVp, intensity of 145 µA, integration time of 300 ms and at an isotropic voxel size of 6 µm. In tibias, Regions of Interest (ROIs) for (a) Metaphyseal, (b) Trabecular and (c) Cortical bone analysis are defined based on three anatomical landmarks, visualized by scanned images: 1) End of Growth Plate; 2) Crest of Tibia; 3) Tibia-fibula junction. (a) Metaphyseal bone's ROI has been defined as the region between the Landmark 1 and Landmark 2. Metaphyseal bone analysis has been performed by evaluating 12.5 % of the scanned images from the End of Growth Plate toward to Crest of Tibia. (b) Trabecular bone's ROI has been defined as the region between the Landmark 1 and Landmark 2. Trabecular bone analysis has been performed by evaluating 12.5 % of the scanned images from the end of growth plate toward to crest of tibia. (c) Cortical bone's ROI has been defined as the region between Landmark 2 and Landmark 3. Cortical bone analysis has been performed by evaluating 6.25 % of the scanned images above and below from the midshaft toward to Crest of Tibia and Tibia-fibula junction, respectively (Suppl. Fig. 2A). In femurs, ROIs for (a) Metaphyseal, (b) Trabecular and (c) Cortical bone analysis are defined based on three anatomical landmarks, visualized by scanned images: 1) Articular Cartilage Surface; 2) End of Growth Plate; 3) Middle area Lesser Trochanter-Third Trochanter. (a) Metaphyseal and (b) Trabecular bone analysis were performed by evaluating 6.5% of the scanned slices from Landmark 2 toward Third Trochanter. (c) Cortical bone analysis was performed by evaluating 6.25% of the scanned slices from the middle area toward Landmark 1 (Suppl. Fig. 2B). In ROIs, we evaluated with a

direct-model morphometric measure the following parameters, as reported [87]: (a) BV/TV, Thickness, Area, mg HA/BV cm<sup>3</sup>; (b) Tb.N., Tb. Th., Tb. Sp., BV/TV, mg HA/BV cm<sup>3</sup>; (c) Thickness, Area, BV/TV, mg HA/BV cm<sup>3</sup>. In metaphyseal and cortical bone analysis, reconstructed  $\mu$ CT cross-section images were manually double-contoured in ROIs, to include only bone structures. Medullary space and the space external to the periosteal surface were excluded. Gaussian segmentation filter with kernel of 2, standard deviation of 1.2 voxels and range of threshold (220–1000) were uniformly applied to the volume of interest during analysis, as reported. [87] Results presented are divided by the number of slices encompassing the ROI to normalize for varying region size.

## 2.5. Micro-computed tomography analysis of fracture calluses

Calluses from males IGF-1R<sup>lckO</sup> (indKO) and control (Con) mice were used for  $\mu$ CT analysis. Native scans were performed in 70 % ethanol at 55 kVp, 145  $\mu$ A, 300 ms integration time, and at 6- $\mu$ m isotropic voxel edge along a length of the tibia centered on the fracture line. Volumetric analysis of tissue composition was measured only in the callus by narrowing the analysis from the first metaphyseal to the last distal sign (indicated by periosteal enlargement) of the callus formation when examining the coronal plane of the  $\mu$ CT images, as reported. [54,86] Further narrowing to within the fracture line was done by including only areas with signs of breaking within the cortical bone in the transversal plane, as reported. [54,86] In this region, we evaluated with a direct-model morphometric measure of bone volume (BV) over total volume (TV), and mg HA/BV cm<sup>3</sup> segmentation was performed based on a calibration curve derived from manufacturer-supplied phantoms containing known hydroxyapatite (HA) composition: voxels with a linear attenuation coefficient  $\geq 1.76$  cm<sup>-1</sup> (corresponding to 330 mg HA/cm<sup>3</sup>) were considered mineralized tissue. A Gaussian segmentation filter with kernel of 2 and standard deviation of 1.2 voxels was uniformly applied to the volume of interest. Within the mineralizing callus, different ranges of thresholds were identified based on a parametric thresholding study obtained by  $\mu$ CT scanning, described previously (Low mineralized tissue = 410–570; High mineralized tissue = 570–1000). [53,54] Results presented are volumes of each threshold range divided by the number of slices encompassing the callus to normalize for varying callus size. Soft tissues were evaluated by using a post-mortem phosphotungstic acid (PTA) contrast-enhanced scanning that allows a better visualization of soft tissue through PTA-collagen binding at basic amino side chains. [53,88] Samples were stained with 5 % PTA in 70 % ethanol for 14 days before scanning. The volume of soft tissue in the callus was obtained by subtracting the volume of total mineralized tissue from the total tissue volume measured with contrast-enhanced scanning (Threshold = 180–410).

## 2.6. Staining and immunofluorescence studies

Whole-mount Alizarin red/Alcian blue staining was performed as previously reported. [89] Images were taken using a stereo microscope (SZX16; Olympus) equipped with a digital camera (DP71; Olympus) and imported into Photoshop (Adobe). Tibias from at least five individual animals per time point per study were dissected and subjected to staining or immunofluorescence (IF) analysis. Tibias were fixed in 4 % paraformaldehyde for 18 h, then decalcified in 14 % EDTA solution for 14–21 days before embedding in paraffin, or soaked in 30 % sucrose for approximately 24–48 h and embedded in OCT. Both paraffin- and OCT-embedded tissues were sectioned at 6  $\mu$ m. Both paraffin- and cryo-sectioned tibias were subjected to Safranin O/Orange G staining. In fractured tibias, the center of the fracture gap was identified as the largest diameter of the callus in which the fracture line was clearly seen following a serial Safranin O/Orange G staining. All further histological analyses were performed within 500  $\mu$ m of the center of the fracture line. For IF, to mitigate autofluorescence, sections were pretreated with 1 % NaBH<sub>4</sub> for 20 min, blocked for endogenous mouse IgG using M.O.M

Kit (Mouse on Mouse Kit, Jackson ImmunoResearch) combined with 5 % normal donkey serum (NDS) for 1 h and incubated in primary antibodies in 2 % NDS buffer overnight at room temperature; sections were incubated in the appropriate secondary antibody diluted in 2 % NDS buffer for 1 h. Sections were counterstained with DAPI for nuclear staining and mounted with Aquamount (ThermoFisher). As a control, sections were processed with the omission of primary antibodies. The list of used primary and secondary antibodies is reported in Supplemental Table 2. Images were taken with either an Olympus BX60 Microscope with a DP71 camera or an Olympus VS120 with a 60 $\times$  PlanApo oil immersion lens zoomed 2 $\times$  using sequential scanning. Images were viewed with Olympus FV10-ASW Viewer software and final images merged with Photoshop.

## 2.7. Quantification of positive cells

For IF analysis, at least six sections per animal and 3–5 animals per genotype were analyzed and examined. Unfractured tibia from IGF-1R<sup>lckO</sup> mice and calluses from IGF-1R<sup>lckO</sup> mice, as well as their controls, were sectioned (6  $\mu$ m), stained and imaged using a predetermined area (50  $\times$  50  $\mu$ m). Immunofluorescence-label positive cells were counted in each predetermined area and in each section and reported as the relative number of positive cells of the total number of cells [(% positive cells/DAPI<sup>+</sup> cells)  $\pm$  SD].

## 2.8. Bone histomorphometry analysis

Tibias from 8 weeks-old males and females IGF-1R<sup>lckO</sup> and control mice were harvested, fixed in 70 % ethanol and shipped to Pathology Core Research Lab at University of Alabama at Birmingham for *in-vivo* bone histomorphometry analysis. [90] For dynamic bone histomorphometry measurements, Calcein Green (7,5 mg/kg BW) and Alizarin Red complexone (30 mg/kg BW) (Sigma-Aldrich, St Louis, MO, USA) were (*i.p.*)-injected for fluorochrome labelling of the bone on Day 9 and Day 2, respectively, before the mice were sacrificed (Fig. 1G).

## 2.9. Endosteal cell isolation

Endosteal cells were freshly isolated from long bones of 8–10 weeks-old IGF-1R<sup>lckO</sup> and control mice, by using the procedure of Balduino et al. [91,92], as we previously reported. [12,53] Briefly, intact tibias and femurs were dissected, all extraneous connective and muscle tissues were carefully removed, and then treated with five incubations 30 min/each in 0.1% collagenase and 0.125% trypsin in Hank's balanced salt solution, after the digestions the periosteal sites were mechanically scraped, in order to remove the adherent cells from the periosteum. Although we can't exclude that some residual periosteal cells were still after isolation, we consider that enzymatic digestions and mechanical scraping should have removed the vast majority of the cells. BM was then removed by flushing and bones were broken into segments and treated twice with 0.1 % collagenase for 40 min at 37 °C in order to isolate endosteal cells. Cells were grown in Dulbecco's modified Eagle's medium with antibiotics and 10 % fetal bovine serum (Atlanta Biologicals) as maintenance media to allow confluence (undifferentiated conditions). Cells were grown at 37 °C and 5 % CO<sub>2</sub> for three passages before being used for experiments. Osteoblastic differentiation was carried out using StemXVivo osteogenic base media plus 0.5 $\times$  StemX-Vivo osteogenic supplement (R&D Systems). Media was changed every three days for the length of the experiment. Mineralization was determined by staining with a 2 % solution of Alizarin red for 15 min following fixation in formalin. To quantify the Alizarin Red staining, 10% cetylpyridinium chloride (Sigma Aldrich) was added (1 ml for 10 cm<sup>2</sup>) and cells were incubated for 20 min to elute the stain. Alizarin Red staining was then quantified by measuring the absorbance of the eluted stain at 570 nm using a spectrophotometer and normalizing by the number of cells (counted in unstained wells that were prepared in

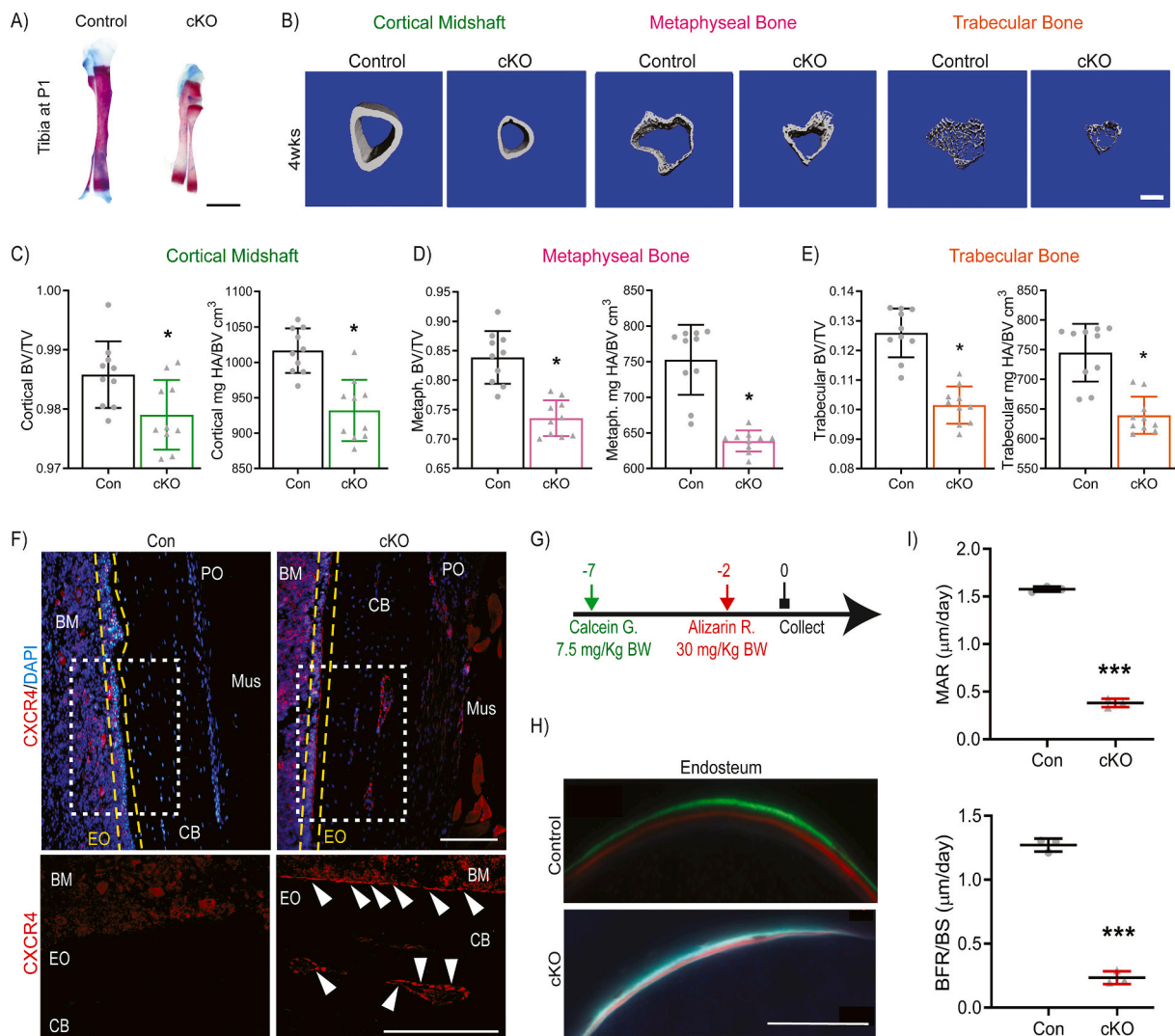


**Fig. 1.** IGF-1R<sup>CKO</sup> mice show defective bone mineralization and formation and an increase of CXCR4 endosteal expression. (A) Alcian Blue-Alizarin Red staining of tibia from IGF-1R<sup>CKO</sup> (cKO) and *Igf1r<sup>fl/fl</sup>* (Control) at postnatal Day 1 (P1). Scale bar = 100  $\mu$ m. (B) Representative  $\mu$ CT three-dimensional images of IGF-1R<sup>CKO</sup> (cKO) and control (Con) tibias (Cortical Midshaft, Metaphyseal Bone and Trabecular Bone) obtained from 4-week old mice. Scale bar = 1 mm. (C)  $\mu$ CT analysis of the Cortical BV/TV, mg HA/BV cm<sup>3</sup>, (D) Metaphyseal BV/TV, mg HA/BV cm<sup>3</sup>, (E) Trabecular BV/TV, mg HA/BV cm<sup>3</sup>. All data are normalized to the number of slices comprising the ROI and are reported as mean  $\pm$  SD. N = 11. \*,  $p < 0.05$ , \*\*,  $p < 0.01$ , compared to Con by unpaired two-tail *t*-test. (F) Representative IF images of IGF-1R<sup>CKO</sup> (cKO) and control (Con) mice at 28 postnatal days, immunostained with CXCR4 antibody, counterstained with DAPI. White arrows indicate areas with CXCR4<sup>+</sup> cells. Yellow dotted lines identify the endosteum. Mus = muscle; BM = bone marrow; PO = periosteum; EO = endosteum. Scale bars = 100  $\mu$ m. (H) Schematic representation of Calcein Green and Alizarin Red complexone injections for *in vivo* histomorphometry analysis performed in 8 week-old male IGF-1R<sup>CKO</sup> (cKO) and control mice. (I) Representative IF images of histomorphometry analysis indicating the new bone formation front respectively in IGF-1R<sup>CKO</sup> (cKO) and control (Con) mice. N = 3. Scale bars = 500  $\mu$ m. (I) Dynamic data (BFR/BS; MAR) of the *in vivo* histomorphometry analysis. Data are reported as mean  $\pm$  SD. N = 3. \*\*\*,  $p < 0.001$ , compared to Con by unpaired two-tail *t*-test. (For interpretation of the references to color in this figure legend, the reader is referred to the web version of this article.)

parallel). For *in vitro* AMD3100 treatment of confluent endosteal cell cultures, osteogenic differentiation was initiated as described above; beginning on day 7, 400  $\mu$ M AMD3100 was added to the cultures every 3 days until day 14, when cells were harvested.

## 2.10. mRNA isolation and qRT-PCR

mRNA was collected from cells using the mMACS mRNA Isolation kit (Miltenyi Biotec, San Diego, CA, USA). Contaminating DNA was removed with DNase I (New England BioLabs, Ipswich, MA, USA) and extracted mRNA was converted to cDNA using mMACS One-Step cDNA Kit (Miltenyi Biotec). To determine the expression of marker genes, we performed qRT-PCR using PowerUp SYBR Green Supermix and StepOnePlus™ Real-Time System and StepOne™ software (Applied

Biosciences, Beverly Hills, CA, USA). Analysis of relative gene expression was made using the Pfaffl method with GAPDH as housekeeping gene. Primers are reported in Supplemental Table 1.

## 2.11. Biomechanical testing analysis

Calluses from IGF-1R<sup>CKO</sup> and control mice at PFD 14 and PFD 21, treated with AMD3100 or PBS, were subjected to distraction-to-failure tension biomechanical testing (BMT). As reported [86], the bone ends were potted with polymethylmethacrylate and loaded into the Electro-force system ELF 3200 (Bose Corporation, Framingham, MA, USA). The displacement rate was set at 0.25 mm/min and a force displacement curve recorded to calculate the ultimate force (maximum force at failure) and stiffness (maximum slope) using WinTest Control software.

## 2.12. Statistical analysis

All quantitative experiments have at least 3 independent biological replicates. Results are presented as mean  $\pm$  SD. For cell culture, each experiment included 3–5 samples. Statistical analysis were performed in GraphPad Prism 9, using a two-tailed unpaired Student's *t*-test for single comparisons or one-way ANOVA followed by Tukey's test for multiple comparisons. Statistical significance was set at  $p \leq 0.05$ .

## 3. Results

### 3.1. Long-bone mineralization defects associated with altered expression of CXCR4 in postnatal IGF-1R<sup>CKO</sup>

To conditionally inactivate IGF-1R in osteochondroprogenitors, we crossed *Igf1r<sup>fl/fl</sup>* homozygous females with *Prx1-Cre<sup>+</sup>;Igf1r<sup>fl/-</sup>* males heterozygous for the *Igf1r<sup>fl</sup>* allele and carrying the *Prx1-Cre* transgene to generate *Prx1-Cre<sup>+</sup>;Igf1r<sup>fl/fl</sup>* (hereafter called IGF-1R<sup>CKO</sup>) mice. IGF-1R<sup>CKO</sup> animals showed shorter and demineralized hindlimbs (Fig. 1A) and overall skeletons (Suppl. Fig. 1), a phenotype that was noted at birth and persisted at 6 weeks of age. Since the main purpose of our studies was the study of long-bone fracture repair, we focused our investigation on tibias, a main site of non-union. [47] We quantified the demineralization of IGF-1R<sup>CKO</sup> tibias by  $\mu$ CT analysis using well defined landmarks (described in Materials & methods and Suppl. Fig. 2). As shown in Fig. 1B–C–D–E, compared to control (*Igf1r<sup>fl/fl</sup>*) tibias and femurs at 4 weeks-old, IGF-1R<sup>CKO</sup> male mice showed a decrease in BV/TV and mg HA/BV cm<sup>3</sup> in the cortical, metaphyseal and trabecular bone regions; they also displayed a decrease in trabecular number (Tb.N.), thickness (Tb. Th.) and separation (Tb. Sp.) (Suppl. Fig. 3, Suppl. Fig. 4). Notably,  $\mu$ CT analysis performed in 4, 8, and 12 weeks-old male mice indicated that the bone structural defects in IGF-1R<sup>CKO</sup> mice persisted with age (Suppl. Fig. 3, Suppl. Fig. 4). Similar results were found in female IGF-1R<sup>CKO</sup> mice when compared with age- and sex-matched control mice (Suppl. Fig. 5). Remarkably, IF analyses showed that tibias of IGF-1R<sup>CKO</sup> mice had an increased number of lining endosteal cells expressing CXCR4 (CXCR4<sup>+</sup>/DAPI<sup>+</sup> = 82.26 %  $\pm$  0.49; N = 4.  $p < 0.05$ ), compared to controls (CXCR4<sup>+</sup>/DAPI<sup>+</sup> = 12.21 %  $\pm$  0.27; N = 4.  $p < 0.05$ ) (Fig. 1F). Furthermore, H&E staining of tibias from IGF-1R<sup>CKO</sup> mice showed an increase of vascular-like structures within the demineralized cortical bone, indicative of increased angiogenesis (Suppl. Fig. 6A). IF analysis detected CXCR4<sup>+</sup> cells within the vascular-like structures in the abnormal cortical bone in mutant mice (Fig. 1F), as well as CD31<sup>+</sup> cells (Suppl. Fig. 6B), confirming that the structures were endothelial in nature. In contrast, neither CXCR4<sup>+</sup> nor CD31<sup>+</sup> cells were present in tibias of control mice (Suppl. Fig. 6B). To further evaluate the IGF-1R<sup>CKO</sup> bone phenotype, we performed *in vivo* histomorphometry analysis in 8 weeks-old male IGF-1R<sup>CKO</sup> and control mice. For this purpose, Calcein Green and Alizarin Red were intraperitoneally (*i.p.*)-injected 9 and 2 days before euthanasia, respectively (Fig. 1G). Compared to controls, IGF-1R<sup>CKO</sup> mice showed a decrease in new bone endosteal formation, as well as decreases in both mineral apposition rate (MAR) and bone formation rate (BFR) (Fig. 1H–I). Notably, we found similar results in female IGF-1R<sup>CKO</sup> mice (data not shown).

Taken together, our data have shown that the conditional ablation of IGF-1R in osteochondroprogenitors led to long-bone mineralization and formation defects, associated with increased expression of CXCR4 within the endosteum and in vascular-like structures within the cortical bone.

### 3.2. CXCR4 mediates the effects of IGF-1R signaling in maintaining bone homeostasis

To mechanistically evaluate whether the altered CXCR4 expression pattern in IGF-1R<sup>CKO</sup> endosteal cells has a functional role on their osteogenic differentiation capability, primary endosteal cells from hindlimb

long-bones of IGF-1R<sup>CKO</sup> and control mice (6–8 weeks old) were isolated and cultured in osteogenic medium for 14 days. In isolated IGF-1R<sup>CKO</sup> endosteal cells, we noted a decreased mRNA expression of osteogenic markers (Runx2, Osx, Col1) when compared to control cells (Fig. 2B). Alizarin Red staining (including semi-quantitative analysis) confirmed a failure in the differentiation and mineralization processes in IGF-1R<sup>CKO</sup> endosteal cells compared to controls (Fig. 2C; Suppl. Fig. 7A). Furthermore, when compared to controls, isolated IGF-1R<sup>CKO</sup> endosteal cells showed increased mRNA expression of pericyte markers ( $\alpha$ SMA, NG2, PDGFR $\beta$  and Prx1) (Suppl. Fig. 7B). Remarkably, in isolated IGF-1R<sup>CKO</sup> endosteal cells, the failure of mineralization was associated with an increase in both CXCR4 and CXCL12 expression (Fig. 2D).

To investigate whether the increased expression of CXCR4/CXCL12 in IGF-1R<sup>CKO</sup> endosteal cells plays a functional role in inhibiting their differentiation potential, we treated IGF-1R<sup>CKO</sup> endosteal cells with AMD3100, a pharmacological antagonist of CXCR4. As schematically shown in Fig. 2A, cells received treatment with AMD3100 at a dose of 400  $\mu$ M every 3 days from day 7 to day 14 during osteogenic differentiation. AMD3100 corrected the osteogenic differentiation defects of IGF-1R<sup>CKO</sup> endosteal cells, as indicated by the increase in osteogenic marker expression and Alizarin Red staining (Fig. 2B–D; Suppl. Fig. 7A).

Furthermore, in IGF-1R<sup>CKO</sup> endosteal cells AMD3100 increased expression of pericyte markers (Suppl. Fig. 7B). Notably, in control cells AMD3100 had no effect on the expression of Runx2, Col1, NG2, PDGFR $\beta$ , and Alizarin Red staining, and it slightly decreased Osx,  $\alpha$ SMA and Prx1 expression. Interestingly, AMD3100 decreased CXCR4 and CXCL12 expression in IGF-1R<sup>CKO</sup> endosteal cells, but not in control cells (Fig. 2C). These findings are consistent with previous studies reporting that AMD3100 can decrease CXCR4/CXCL12 expression through a desensitization/internalization process. [48–51]

Next, we pursued *in vivo* studies, in which we treated IGF-1R<sup>CKO</sup> and control mice with AMD3100. Mice were subcutaneously (*s.c.*)-injected every other day with an AMD3100-PBS solution (2.5 mg/g of BW per injection) from postnatal day 3 to postnatal day 28, at which point animals were euthanized (Fig. 2E). We found that AMD3100 treatment overall either normalized or greatly improved the bone defects in IGF-1R<sup>CKO</sup> mice (Fig. 2F), and had positive effects in tibia and femurs in increasing: [a] metaphyseal BV/TV (Fig. 2G, Suppl. Fig. 9A), Area, Thickness and mg HA/BV cm<sup>3</sup> (Suppl. Fig. 8A, Suppl. Fig. 9A); [b] cortical BV/TV (Fig. 2G), Area, Thickness and mg HA/BV cm<sup>3</sup> (Suppl. Fig. 8B, Suppl. Fig. 9B); [c] trabecular BV/TV, mg HA/BV cm<sup>3</sup>, Tb.N., Tb. Th., and Tb. Sp., (Suppl. Fig. 8C, Suppl. Fig. 9C). Remarkably, IF analysis showed that in IGF-1R<sup>CKO</sup> mice, AMD3100 decreased the number of CXCR4<sup>+</sup> cells in the endosteum and within the cortical bone (CXCR4<sup>+</sup>/DAPI<sup>+</sup> = 11.23 %  $\pm$  0.61; N = 3.  $p < 0.05$ ) (Fig. 2H). Consistent with this observation, AMD3100 also decreased CXCR4 mRNA expression in the tibias of IGF-1R<sup>CKO</sup> mice (Fig. 2I). Furthermore, we noted that AMD3100 affected the abnormal angiogenesis in IGF-1R<sup>CKO</sup> mice as indicated by a decrease in CD31 expression (Fig. 2I).

Taken together, our *in vitro* and *in vivo* data have demonstrated that IGF-1R signaling regulates bone homeostasis by modulating the expression and signaling of CXCR4/CXCL12, a critical pathway for maintaining normal bone integrity.

### 3.3. Tight regulation of CXCR4 by IGF-1R signaling is critical to promote the fracture repair process

We studied the crosstalk between IGF-1R signaling and CXCR4 in fracture repair by using a semi-stabilized tibia fracture model in which intramedullary fixation enables relative stability to facilitate endochondral ossification. [52] For this purpose, we conditionally induced the ablation of IGF-1R via 4OH-TAM administration right before and during the fracture process by crossing male *Prx1CreER-GFP<sup>+</sup>/Igf1r<sup>fl/-</sup>* heterozygous mice with female *Igf1r<sup>fl/fl</sup>* mice to obtain *Prx1CreER-GFP<sup>+</sup>/Igf1r<sup>fl/fl</sup>* (hereafter called IGF-1R<sup>lckO</sup>) mice. IGF-1R<sup>lckO</sup> mice and littermate controls received 4OH-TAM for 5 consecutive days (0.5  $\mu$ g/g

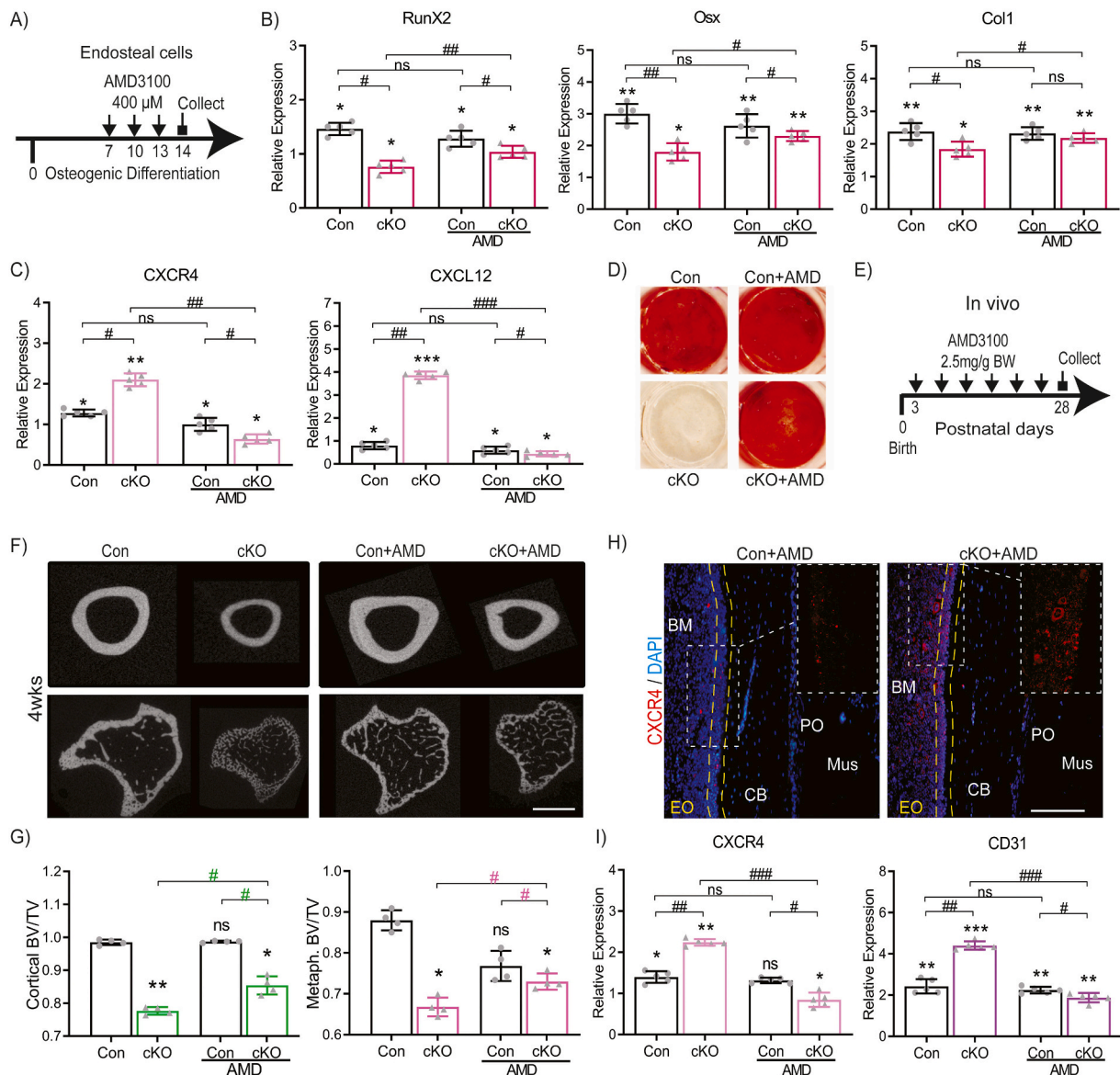


**Fig. 2.** *In vivo* and *in vitro* AMD3100 treatment rescues defective osteogenic differentiation and altered CXCR4 expression pattern in both endosteal cells and endosteum in IGF-1R<sup>ckO</sup> mice.

(A) Schematic representation of AMD3100 treatment in isolated endosteal cell from IGF-1R<sup>ckO</sup> and control mice during osteogenic differentiation. (B) mRNA expression levels quantified by qRT-PCR of osteogenic markers (RunX2, Osx, Col1), (C) CXCR4 and CXCL12, treated with and without AMD3100, at 14 days of osteogenic induction. Data are reported as mean  $\pm$  SD of triplicate repeats from N = 5. \*,  $p < 0.05$ , \*\*,  $p < 0.01$ , \*\*\*,  $p < 0.001$ , compared to Day 0=1Con by one-way ANOVA and Tukey's multiple comparison test. #,  $p < 0.05$ , ##,  $p < 0.01$ , ###,  $p < 0.001$ , by unpaired two-tail *t*-test. ns = not significant. (D) Alizarin Red staining. (E) Schematic representation of AMD3100 *s.c.*-injections in IGF-1R<sup>ckO</sup> and control mice. (F) Representative  $\mu$ CT bi-dimensional images from males IGF-1R<sup>ckO</sup> (cKO) and control (Con) mice at postnatal day 28, treated with and without AMD3100. Scale bar = 1 mm. (G) Cortical and Metaphyseal BV/TV are normalized to the number of slices comprising the ROI. Data are reported as mean  $\pm$  SD. N = 4. \*,  $p < 0.05$ , \*\*,  $p < 0.01$ , compared to Con by one-way ANOVA and Sidak's multiple comparison test. #,  $p < 0.05$ , by unpaired two-tail *t*-test. ns = not significant. (H) Representative IF images of AMD3100-treated IGF-1R<sup>ckO</sup> (cKO + AMD) and control (Con + AMD) mice at postnatal day 28, immunostained with CXCR4 antibody, counterstained with DAPI. Yellow dotted lines identify the endosteum. White dotted lines indicate magnified area. Mus = muscle; CB = cortical bone; BM = bone marrow; PO = periosteum; EO = endosteum. Scale bars = 100  $\mu$ m. (I) mRNA expression levels quantified by qRT-PCR of CXCR4 and CD31 in unfractured tibias from IGF-1R<sup>ckO</sup> (cKO) and control (Con) mice, treated with and without AMD3100, at postnatal day 28. Data are reported as mean  $\pm$  SD of duplicate repeats from N = 5 samples.  $p < 0.05$ , \*\*,  $p < 0.01$ , \*\*\*,  $p < 0.001$ , compared to Day 3=1 by one-way ANOVA and Tukey's multiple comparison test. ##,  $p < 0.01$ , ###,  $p < 0.001$ , by unpaired two-tail *t*-test. ns = not significant. (For interpretation of the references to color in this figure legend, the reader is referred to the web version of this article.)

of BW, starting 2 days before the fracture), and calluses were collected at post-fracture day (PFD) 0, 1, 7, 14 and 21 (Fig. 3A).  $\mu$ CT-Phosphotungstic acid (PTA) analysis (that allow visualization and quantification of soft and mineralized tissue) showed that at PFD 14, when compared to control mice (littermates Prx1CreER-GFP<sup>-/-</sup>/Igf1<sup>R/R</sup> that received 4OHTAM), IGF-1R<sup>ckO</sup> had a smaller callus with reduced Total Callus, Soft tissue, Low- and High-mineralized volumes (Fig. 3B–D). Further

supporting a defect in the repair process, biomechanical testing indicated that calluses from IGF-1R<sup>ckO</sup> mice had decreased ultimate force and stiffness, compared to controls (Fig. 3E).

Consistently with the  $\mu$ CT-PTA analysis, Saf O/Orange G staining of sequential histological callus sections (from medial to lateral side) showed that calluses from IGF-1R<sup>ckO</sup> mice exhibited a reduced formation of both cartilaginous callus and new bone (Suppl. Fig. 10). When

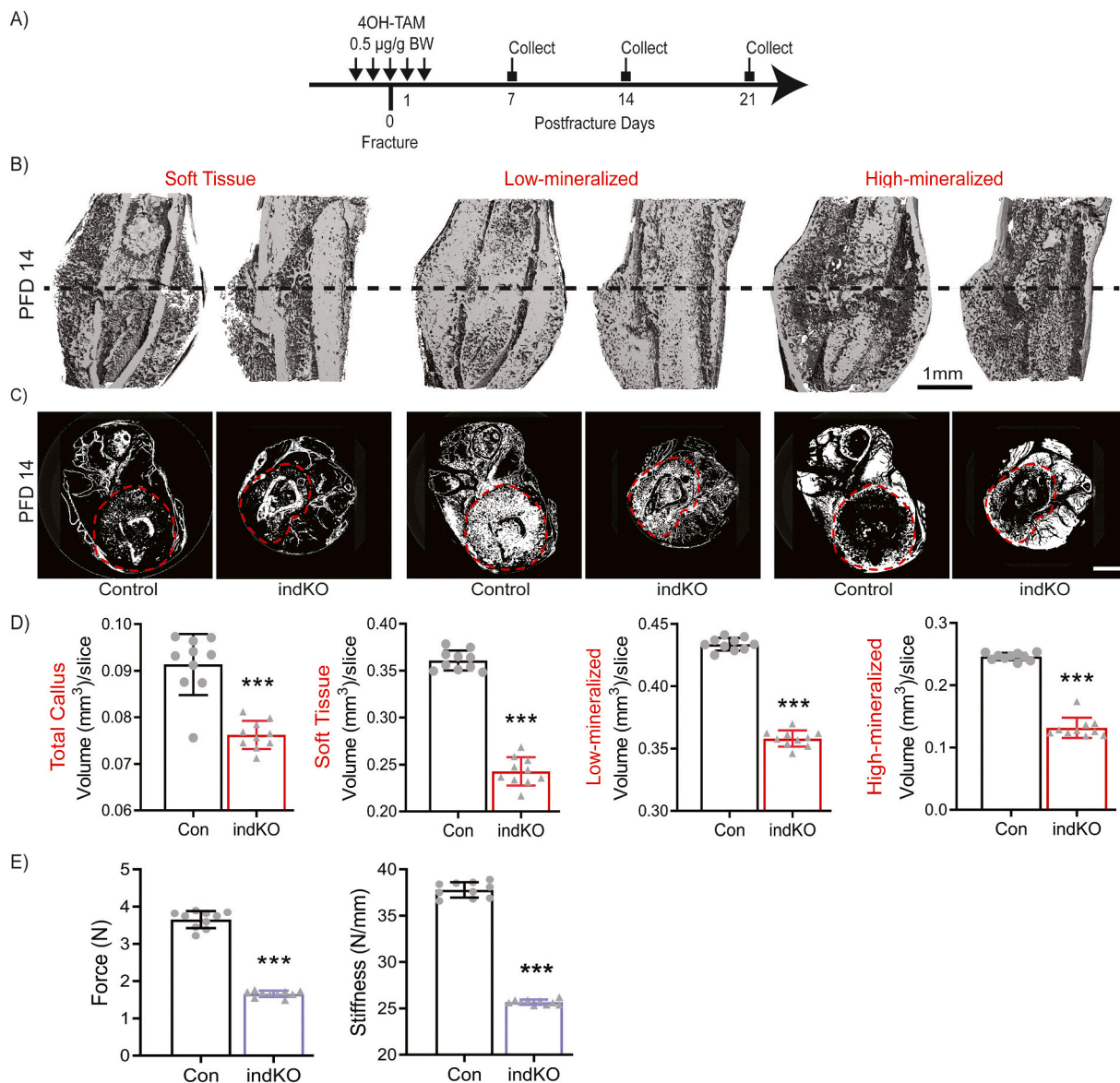


**Fig. 3.** Impaired fracture healing in IGF-1R<sup>IcKO</sup> mice.

(A) Schematic representation of 4OH-TAM *i.p.* injections in fractured IGF-1R<sup>IcKO</sup> and control mice. (B) Representative  $\mu$ CT 3D and (C) bidimensional images from fractured IGF-1R<sup>IcKO</sup> (indKO) and control (Con) mice at PFD 14, with PTA staining. Black dotted line indicates the center of the callus, represented by bidimensional images. Red dotted lines indicate ROIs. Scale bar = 1 mm. (D) Volumes of Total Callus, Soft Tissue, Low- and High-mineralized callus are normalized to the number of slices (mm<sup>3</sup>/slice) comprising the callus. Data are reported as mean  $\pm$  SD. N = 10 samples. \*\*\*,  $p < 0.001$ , compared to Day 14 Con by unpaired two-tail *t*-test. (E) Results for distraction-to-failure biomechanical test for callus Stiffness and Ultimate Force from fractured IGF-1R<sup>IcKO</sup> (indKO) and control (Con) mice at PFD 14. N = 10. Data are reported as mean  $\pm$  SD. \*\*\*,  $p < 0.001$ , compared to Day 14 Con by unpaired two-tail *t*-test. (For interpretation of the references to color in this figure legend, the reader is referred to the web version of this article.)

analyzing sections obtained from the center of the callus, we observed that the scarcely formed callus of IGF-1R<sup>IcKO</sup> mice was mostly constituted of intramembranous woven bone tissue with notable vascular-like structures (Suppl. Fig. 11). Notably, in IGF-1R<sup>IcKO</sup> mice the impairment of healing persisted at PFD 21, when the mutant mice continued to show a reduced mineralization of the callus, a still open fracture line, and biomechanical testing indicated reduced ultimate force and stiffness (Suppl. Fig. 12).

We previously characterized a fracture-induced population of Prx1<sup>+</sup> cells that is critical in initiating the fracture repair process. [53] In the Prx1-CreER-GFP mouse, GFP expression is driven by a 2.4 kb-Prx1 enhancer allowing detection of Prx1-GFP<sup>+</sup> cells that are actively expressing Prx1-Cre and likely have the ability to induce *Cre*-mediated gene recombination. IF analyses for GFP and IGF-1R at PFD 14 indicated

that within the callus of control mice (Prx1CreER-GFP<sup>+</sup>/Igf1r<sup>f/f</sup> fractured mice that did not receive 4OH-TAM) Prx1-GFP<sup>+</sup> expressing cells co-expressed IGF-1R (GFP<sup>+</sup>-IGF-1R<sup>+</sup>/DAPI<sup>+</sup> = 93.14%  $\pm$  0.37; N = 3.  $p < 0.05$ ) (Suppl. Fig. 13A). Indicative of Prx1-Cre recombination efficiency, in IGF-1R<sup>IcKO</sup> mice we noted a drastic and consistent decrease in mRNA expression levels of IGF-1R from PFD 0 to PFD 14 (Suppl. Fig. 13B). Furthermore, in IGF-1R<sup>IcKO</sup> mice double-positive cells were drastically reduced (GFP<sup>+</sup>-IGF-1R<sup>+</sup>/DAPI<sup>+</sup> = 8.38%  $\pm$  0.83; N = 3;  $p < 0.05$ ) (Suppl. Fig. 13C).

In IGF-1R<sup>IcKO</sup> mice, the fracture healing defect was associated with an abnormal callus expression pattern of CXCR4. As shown in Fig. 4A, in the control mice the expression of CXCR4 gradually increased during the first 7 days post-fracture, then drastically dropped by day 14. By contrast, in the IGF-1R<sup>IcKO</sup> mice CXCR4 expression remained high

throughout the fracture healing process and at day 14 was nearly 10-fold higher than expression detected in controls (Fig. 4A). While in IGF-1R<sup>lckKO</sup> mice CXCR4 expression remained high, osteogenic markers (RunX2, Osx, Col1, Ocn; Fig. 4B) and cartilaginous markers (Sox9, Col10, Col2; Fig. 4C) were decreased (consistent with the  $\mu$ CT-PTA analysis presented above). Furthermore, in IGF-1R<sup>lckKO</sup> mice, we found an increase in the expression levels of pericyte markers ( $\alpha$ SMA, NG2, PDGFR $\beta$ , Prx1; Fig. 4D), as well as endothelial markers (CD31; Fig. 4F). IF analysis provided further information about the localization of cells that were abnormally expressing CXCR4 in IGF-1R<sup>lckKO</sup> calluses. As shown in Suppl. Fig. 14, in IGF-1R<sup>lckKO</sup> mice, CXCR4<sup>+</sup> cells were detected in the intramembranous region and co-expressed CD31 (CXCR4<sup>+</sup>-CD31<sup>+</sup>/DAPI<sup>+</sup> = 88.46 %  $\pm$  0.76; N = 3.  $p$  < 0.05) and Prx1 (CXCR4<sup>+</sup>-Prx1<sup>+</sup>/DAPI<sup>+</sup> = 72.64 %  $\pm$  0.53; N = 3.  $p$  < 0.05), while they did not co-express Ocn (CXCR4<sup>+</sup>-Ocn<sup>+</sup>/DAPI<sup>+</sup> = 7.82 %  $\pm$  0.34; N = 3.  $p$  < 0.05) and Sox9 (CXCR4<sup>+</sup>-Sox9<sup>+</sup>/DAPI<sup>+</sup> = 11.29 %  $\pm$  0.38; N = 3.  $p$  < 0.05). In control mice, CXCR4<sup>+</sup> cells were mainly detected in the cartilaginous callus and co-expressed Sox9 (CXCR4<sup>+</sup>-Sox9<sup>+</sup>/DAPI<sup>+</sup> = 68.43 %  $\pm$  0.22; N = 3.  $p$  < 0.05), but in the intramembranous callus we found a very limited number of CXCR4<sup>+</sup> cells that did not express either Prx1 (CXCR4<sup>+</sup>-Prx1<sup>+</sup>/DAPI<sup>+</sup> = 15.72 %  $\pm$  0.39; N = 3.  $p$  < 0.05) or Ocn (CXCR4<sup>+</sup>-Ocn<sup>+</sup>/DAPI<sup>+</sup> = 5.37 %  $\pm$  0.13; N = 3.  $p$  < 0.05) (Suppl. Fig. 14). Furthermore, we found that in control mice, CXCR4<sup>+</sup>-CD31<sup>+</sup> cells were drastically reduced in the intramembranous regions (CXCR4<sup>+</sup>-CD31<sup>+</sup>/DAPI<sup>+</sup> = 16.22 %  $\pm$  0.16; N = 3.

$p$  < 0.05) when compared to IGF-1R<sup>lckKO</sup> mice (Suppl. Fig. 14). Lastly, when we performed triple IF staining for CXCR4, GFP and IGF-1R in intramembranous callus of IGF-1R<sup>lckKO</sup> mice at PFD 14, we observed that ~89 % (GFP<sup>+</sup>-IGF-1R<sup>-</sup>-CXCR4<sup>+</sup>/DAPI<sup>+</sup> 88.72 %  $\pm$  0.52; N = 3.  $p$  < 0,05) of the CXCR4<sup>+</sup> cells were IGF-1R<sup>-</sup>/GFP<sup>+</sup> (Suppl. Fig. 15).

Taken together, our studies in IGF-1R<sup>lckKO</sup> mice have indicated that the ablation of IGF-1R in osteochondroprogenitors leads to failure of fracture healing and is associated with increased CXCR4 expression and altered CXCR4 expression pattern in the callus.

### 3.4. AMD3100 restores fracture healing in IGF-1R<sup>lckKO</sup> mice

To further investigate whether the altered expression of CXCR4 in IGF-1R<sup>lckKO</sup> mice could account for the failure in fracture healing, we treated IGF-1R<sup>lckKO</sup> mice with AMD3100 2 days before fracture and from PFD 2 to PFD 7 (Fig. 5A).  $\mu$ CT-PTA quantitative analysis showed that AMD3100-treated IGF-1R<sup>lckKO</sup> mice formed a well-organized callus (Fig. 5B), with normalized Total callus, Soft tissue, Low- and High-mineralized callus volumes (Fig. 5C). Furthermore, AMD3100 improved the biomechanical properties of the callus in IGF-1R<sup>lckKO</sup> mice (Fig. 5D). Consistent with this  $\mu$ CT-PTA quantitative analysis, AMD3100 treatment of IGF-1R<sup>lckKO</sup> mice increased and normalized the expression of bone and cartilage markers (Suppl. Fig. 16A–B), as well as pericyte markers (Suppl. Fig. 16C) and CD31 (Suppl. Fig. 16D). Notably, in IGF-1R<sup>lckKO</sup> mice AMD3100 treatment decreased CXCR4 and CXCL12 mRNA

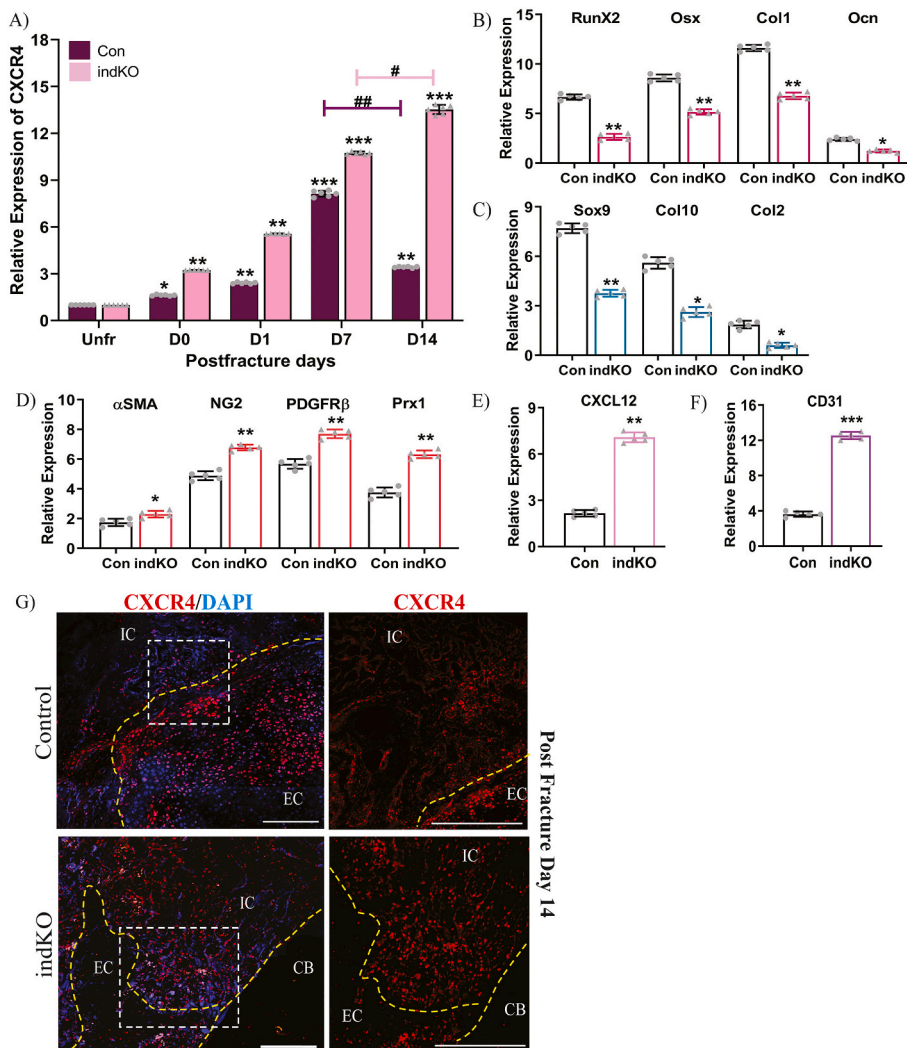


**Fig. 4.** Altered CXCR4 expression in fractured IGF-1R<sup>lckKO</sup> mice.

(A) mRNA expression levels quantified by qRT-PCR of CXCR4 in unfractured (Unfr) and fractured tibias from IGF-1R<sup>lckKO</sup> (indKO) and control (Con) mice. Data are reported as mean  $\pm$  SD of triplicate repeats from N = 6. \*,  $p$  < 0.05, \*\*,  $p$  < 0.01, \*\*\*,  $p$  < 0.001, compared to Unfr=1 by one-way ANOVA and Tukey's multiple comparison test. #,  $p$  < 0.05, ##,  $p$  < 0.01, by unpaired two-tail  $t$ -test. (B–F) mRNA expression levels quantified by qRT-PCR of: (B) osteogenic (RunX2, Osx, Col1, Ocn), (C) chondrogenic (Sox9, Col10, Col2), (D) pericyte markers ( $\alpha$ SMA, NG2, PDGFR $\beta$ , Prx1), (E) CXCL12 and (F) CD31 in fractured IGF-1R<sup>lckKO</sup> (indKO) and control (Con) mice. Data are reported as mean  $\pm$  SD of triplicate repeats from N = 5 samples. \*,  $p$  < 0.05, \*\*,  $p$  < 0.01, \*\*\*,  $p$  < 0.001, compared to Con by unpaired two-tail  $t$ -test. (G) Representative IF images from fractured IGF-1R<sup>lckKO</sup> (indKO) and control (Con) mice at PFD 14, immunostained with CXCR4 antibody and counterstained with DAPI (blue). Yellow dotted lines indicate EC and CB areas. White dotted lines indicate magnified areas. IC = intramembranous callus. EC = endochondral callus. CB = cortical bone. Scale bar = 100  $\mu$ m. (For interpretation of the references to color in this figure legend, the reader is referred to the web version of this article.)

expression in the callus to levels that were similar to controls (Suppl. Fig. 16E). IF analysis supported our findings that in AMD3100-treated IGF-1R<sup>lckKO</sup> mice, treatment reduced the number of CXCR4<sup>+</sup> cells within the intramembranous callus (Suppl. Fig. 17).

AMD3100 effects on IGF-1R<sup>lckKO</sup> mice persisted at later stage of healing.  $\mu$ CT-PTA (Suppl. Fig. 12A–B–C), biomechanical testing (Suppl. Fig. 12D) and qRT-PCR (Suppl. Fig. 18) analysis performed at PFD 21 indicated that AMD3100-treated IGF-1R<sup>lckKO</sup> mice had a healed fracture, with a normal mineralization and a closed fracture line.

We and others have reported a critical role for IRS-1 (a key IGF-1R signaling mediator) in osteoblastic differentiation and fracture healing, as indicated by the healing failure found in Irs1<sup>KO</sup> mice [54–56]. To

further investigate the regulation of CXCR4 expression by IGF-1R signaling, we analyzed the expression pattern of CXCR4 in fractured Irs1<sup>KO</sup> mice. We found that, similarly to IGF-1R<sup>lckKO</sup> fractured mice, fractured Irs1<sup>KO</sup> mice showed a defect in callus formation associated with an increase of CXCR4, CXCL12, CD31, and pericyte markers (NG2,  $\alpha$ SMA, PDGFR $\beta$ , Prx1), and a decrease of both osteogenic (RunX2, Osx, Col1, Ocn) and chondrogenic (Sox9, Col10, Col2) markers (Suppl. Fig. 19A–B–C–D–E) at PFD 14, when compared sex-matched wild-type controls. Consistent with these observations, IF analysis demonstrated that within the scarcely formed intramembranous callus, Irs1<sup>KO</sup> mice had an abnormally increased number of CXCR4<sup>+</sup> cells (CXCR4<sup>+</sup>/DAPI<sup>+</sup> = 72.22 %  $\pm$  0.23; N = 3), compared to wild-type control (CXCR4<sup>+</sup>/

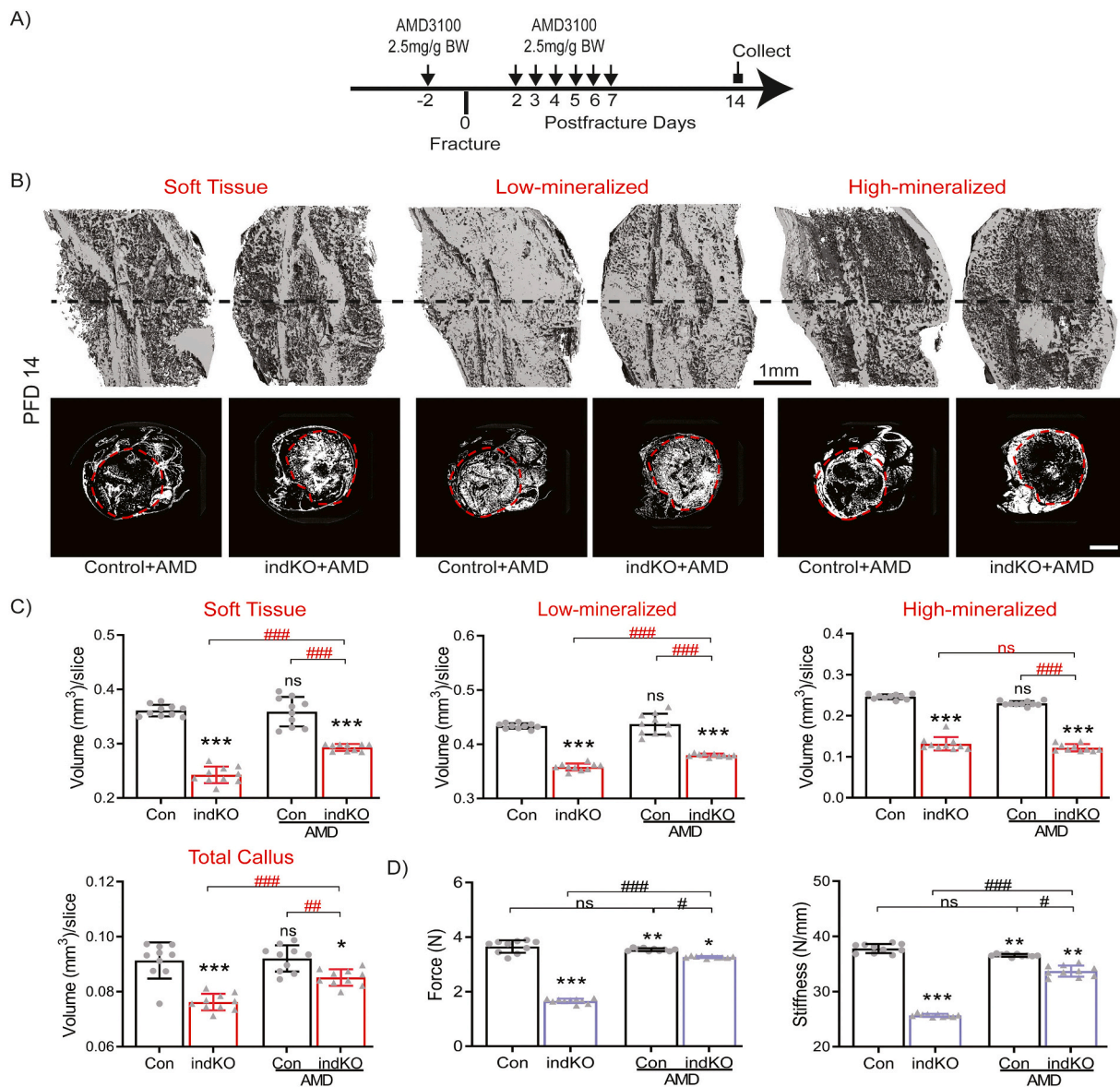


**Fig. 5.** AMD3100 rescues impaired fracture healing in IGF-1R<sup>lckKO</sup> mice.

(A) Schematic representation of AMD3100 *i.p.*-injections in fractured IGF-1R<sup>lckKO</sup> and control mice. (B) Representative  $\mu$ CT 3D and bidimensional images from fractured IGF-1R<sup>lckKO</sup> (indKO) and control (Con) mice at PFD 14, AMD3100-treated (+AMD), with PTA staining. Black dotted line indicates the center of the callus, represented by bidimensional images. Red dotted lines indicate ROIs. Scale bar = 1 mm. (C) Volumes of Total Callus, Soft Tissue, Low- and High-mineralized callus are normalized to the number of slices (mm<sup>3</sup>/slice) comprising the callus. Data are normalized to Unfr and reported as mean  $\pm$  SD. N = 10. \*,  $p < 0.05$ , \*\*\*,  $p < 0.001$ , compared to Con by one-way ANOVA and Tukey's multiple comparison test. #,  $p < 0.01$ , ###,  $p < 0.001$ , by unpaired two-tail *t*-test. ns = not significant. (D) Results for distraction-to-failure biomechanical test for callus Stiffness and Ultimate Force from fractured IGF-1R<sup>lckKO</sup> (indKO) and control (Con) mice at PFD 14, with (AMD) or without AMD3100. Data are reported as mean  $\pm$  SD. N = 10. \*,  $p < 0.05$ , \*\*,  $p < 0.01$ , \*\*\*,  $p < 0.001$ , compared to Con by one-way ANOVA and Tukey's multiple comparison test. #,  $p < 0.05$ , ###,  $p < 0.001$ , by unpaired two-tail *t*-test. ns = not significant. (For interpretation of the references to color in this figure legend, the reader is referred to the web version of this article.)

DAPI<sup>+</sup> = 12.26 % ± 0.24; N = 3; p < 0.05) (Suppl. Fig. 19F).

Taken together, our studies have demonstrated that IGF-1R signaling regulates fracture repair by modulating CXCR4, and a rescue of healing in IGF-1R<sup>ckO</sup> mice can be obtained by timely regulating the expression of CXCR4. Lastly, we found that this regulation can be orchestrated through the IGF-1R/IRS1 signaling pathway.

4. Discussion

In this study, we showed that bone homeostasis and bone fracture healing are controlled by IGF-1R signaling through a tight regulation of appropriate expression levels of CXCR4. Mechanistically, we found that IGF-1R signaling downregulates CXCR4 expression, thus allowing a population of endosteal cells to commit to differentiate into bone cells. By using a combination of *in vivo* and *in vitro* studies, we found that blockage of CXCR4 function by AMD3100 restored the bone defects and improved the fracture healing process in a non-union mouse model with defective IGF-1R signaling. Moreover, we identified the role of IRS1 as a critical intracellular mediator of the osteogenic effects of IGF-1R signaling through the modulation of CXCR4 expression in endosteal cells.

IGF-1 has been reported to play critical roles in development, growth and metabolism. [44,57] *Igf1*<sup>-/-</sup> null mice showed an ~80 % perinatal lethality, and surviving pups were ~50 % smaller than controls, demonstrating a critical role of *Igf1* in embryogenesis. [58]

Heterozygous *Igf1*<sup>-/+</sup> male and female mice displayed reduced body weight, femur length and bone mineral density. [59] Mice with global deletion of the *Igf1* receptor (*Igf1r*<sup>-/-</sup>) had a phenotype similar to *Igf1*<sup>-/-</sup> mice, with pups born smaller than controls and dying shortly after birth. [60] In the fracture healing process, IGF-1/IGF-1R signaling has been shown to induce proliferation and differentiation of osteoprogenitor cells. [26,28,32] Tissue-specific deletion of IGF-1R in osteoblasts [29,38,40], osteocytes [27], chondrocytes [39], and osteoclasts [41] showed reduced cell differentiation and fracture healing. Notably, Wang et al. [38] reported that ablation of IGF-1R signaling in osteoblasts significantly impaired fracture healing, highlighting that IGF-1R signaling was involved in osteoblast differentiation, as well as in coordinating endochondral bone formation during fracture repair. Remarkably, abnormally low levels of circulating IGF-1 have been reported in patients with non-unions. [61] Although this body of evidence supports a key role of IGF-1R signaling in bone formation and repair, its mechanisms of actions and, in particular, the down-stream effectors are still unknown. Here, we report that the absence of IGF-1R signaling in osteochondroprogenitors leads to alterations in the CXCR4 expression pattern that induces low bone mineralization and impairment of fracture healing. Furthermore, we identified a population of IGF-1R<sup>+</sup> endosteal cells that are induced by the fracture-injury process and found that IGF-1R signaling is needed for determining their osteogenic fate. Our findings are summarized in Fig. 6: following a fracture, an IGF-1R<sup>+</sup> endosteal cell population is recruited along the endosteum. A subsequent

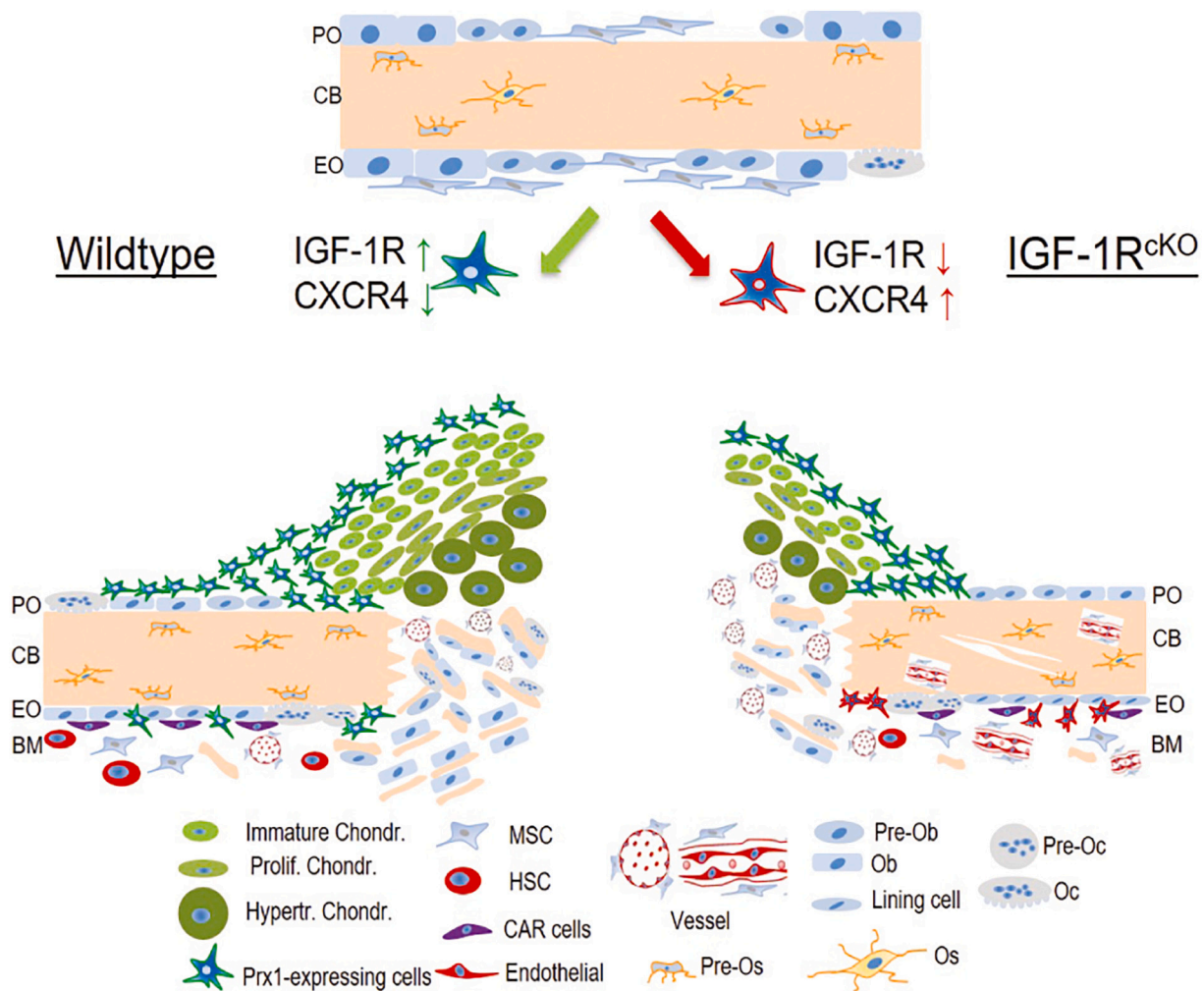


Fig. 6. Graphic model of the functional role of IGF-1R/CXCR4 axis in fracture repair. Following fracture, IGF-1R<sup>+</sup> endosteal cells, are elicited and contribute to the mineralizing callus maturation. IGF-1R signaling at PFD 14 leads to a downregulation of CXCR4, allowing cells to commit to differentiation and callus maturation. In absence of IGF-1R, such regulation of CXCR4 is absent, leading to impaired fracture healing and abnormal angiogenesis.

decrease of CXCR4 by PFD 14 is essential to determine the fate of these cells and trigger differentiation of this endosteal cells population into osteoblasts. In the absence of IGF-1R, the resulting upregulation of CXCR4 leads to healing impairment and abnormal angiogenesis.

CXCR4 is the primary receptor for CXCL12 and both are expressed by different cell types, exerting functions in proliferation, morphogenesis, and migration. [62–64] As a result of their pleiotropic effects, both CXCR4<sup>-/-</sup> and CXCL12<sup>-/-</sup> mice die either *in utero* or perinatally due to multiple defects in the developing brain, intestine, vasculature, heart, and hematopoietic tissues. [65–68] Activated CXCR4/CXCL12 signaling results in the migration of CXCR4-expressing cells toward high concentrations of CXCL12 [65,69–72] and the resulting chemo-attractive mechanism of this CXCL12 gradient is involved in regulating blood cell homeostasis [73], immune response [65], bone remodeling [72], homing of stem/progenitor cells to BM [74], cell recruitment to injured tissues and after BM engraftment. [75–78] Interestingly, Caselli et al. [79] have reported IGF-1R signaling as a mediator of the endosteal niche reorganization and consequently donor BM engraftment. *In vivo* and *in vitro* studies, including from our own laboratory, have reported that CXCR4/CXCL12 signaling stimulates the mobilization of MSCs and osteoprogenitor cells after injury, while inducing their osteogenic differentiation [12,15,78,80] and promoting the fracture repair process. [53,72] The present study delineates *in vivo* a mechanistic regulation of CXCR4 expression in endosteal cells by IGF-1R signaling, and its role in maintaining bone formation and in promoting fracture healing. We found that CXCR4 expression increases during the soft callus formation (from PFD 1 to PFD 7), then decreases along with callus mineralization (PFD 14). Furthermore, in both IGF-1R<sup>CKO</sup> and fractured IGF-1R<sup>CKO</sup> mice, we found that AMD3100 treatment improved the bone mineralization defects and the impaired fracture healing, respectively. Importantly, AMD3100 improved the biomechanical properties of fractured bone in fractured IGF-1R<sup>CKO</sup> mice. The effects of AMD3100 in both IGF-1R<sup>CKO</sup> mice and IGF-1R<sup>CKO</sup> endosteal cells provides mechanistic evidence of the regulation of CXCR4 in committing endosteal cells to differentiation, suggesting a possible variety of avenues for potential therapeutic approaches to treat fracture non-unions, including the pharmacological use of AMD3100. Notably, AMD3100 is FDA-approved for the induction of hematopoietic stem cell mobilization, and it holds an excellent safety profile. [81]

Our *in vivo* and *in vitro* results showed that IGF-1R signaling in the endosteum plays a critical role in this repair process. However, we cannot exclude the possibility that IGF-1R/CXCR4 signaling in other tissues and cell types (such as other cells in the BM) that might also contribute to efficient fracture repair. These questions are beyond the scope of this study and will be addressed in future work.

We and others have reported the critical role of IRS-1 in osteoblastic differentiation of MSCs and showed that Irs1<sup>KO</sup> mice failed fracture healing. [54] Here, we report that similarly to IGF-1R<sup>CKO</sup> mice, the fracture healing impairment in Irs1<sup>KO</sup> mice is associated with abnormal increase in CXCR4 and CXCL12 expression, suggesting that IRS-1 is a mediator by which IGF-1R downregulates CXCR4 in fracture healing.

Periosteal and endosteal cells have been reported to express similar markers, including  $\alpha$ SMA and PDGFR $\beta$  [93–96], and although the extensive enzymatic digestions followed by mechanical scraping should have removed most of the periosteal cells, we can't exclude that residual periosteal cells might have remained in the cell preparation.

Taken together, our identification of a novel population of endosteal cells that is functionally regulated through the modulation of CXCR4 by IGF-1R signaling opens exciting opportunities to explore novel cell-based or pharmacological (*i.e.* AMD3100) therapies to treat non-unions.

Supplementary data to this article can be found online at <https://doi.org/10.1016/j.bone.2022.116600>.

#### CRedit authorship contribution statement

**Alessandra Esposito:** Conceptualization; Data curation; Formal

analysis; Investigation; Methodology; Project administration; Resources; Supervision; Validation; Visualization; Roles/Writing - original draft; Writing - review & editing. **Michael Klüppel:** Formal analysis; Methodology; Review & editing. **Brittany M. Wilson:** Formal analysis; Methodology; Review & editing. **Sai R.K. Meka:** Review & editing. **Anna Spagnoli:** Conceptualization; Data curation; Formal analysis; Funding acquisition; Investigation; Project administration; Supervision; Validation; Visualization; Roles/Writing - original draft; Writing - review & editing.

#### Declaration of competing interest

None.

#### Data availability

Data will be made available on request.

#### Acknowledgements

We acknowledge Dr. Ping Ye at University of North Carolina at Chapel Hill in assisting in the cell-tracing studies. We acknowledge the technical assistance of J.D. Temple for some of the  $\mu$ CT imaging of unfractured mice. We acknowledge the Pathology Core Research Lab of University of Alabama at Birmingham for the technical assistance in histomorphology analysis. We acknowledge the technical assistance of Lily Yu in some of the histological studies. We are grateful to S. Murakami (Case Western Reserve University) for providing the Prx1-CreER transgenic mice and to Dr. C. Ronald Kahn (Joslin Diabetes Center, Boston) for providing the Irs1<sup>KO</sup> mice.

#### Funding

This work was supported by a grant from National Institutes of Health-National Institute of Arthritis and Musculoskeletal and Skin Diseases (1R01AR074049 to A.S.).

#### References

- [1] S.K. Stewart, Fracture non-union: a review of clinical challenges and future research needs, *Malays. Orthop. J.* 13 (2) (2019) 1–10.
- [2] G.B. Reahl, L. Gerstenfeld, M. Kain, Epidemiology, clinical assessments, and current treatments of nonunions, *Curr. Osteoporos. Rep.* 18 (3) (2020) 157–168.
- [3] M. Bonafede, D. Espindle, A.G. Bower, The direct and indirect costs of long bone fractures in a working age US population, *J. Med. Econ.* 16 (1) (2013) 169–178.
- [4] B.G. Dijkman, S. Sprague, M. Bhandari, Low-intensity pulsed ultrasound: nonunions, *Indian J. Orthop.* 43 (2009) 141–148.
- [5] P.V. Giannoudis, C. Tzioupis, Clinical applications of BMP-7: the UK perspective, *Injury* 36 (Suppl 3) (2005) S47–S50.
- [6] A. Praemer, S. Furner, D.P. Rice, Musculoskeletal conditions in the United States. Rosemont: American Academy of Orthopaedic Surgeons. (1999).
- [7] M.F. Pittenger, et al., Mesenchymal stem cell perspective: cell biology to clinical progress, *NPJ Reg. Med.* 4 (2019) 22.
- [8] A. Alhadlaq, J.J. Mao, Mesenchymal stem cells: isolation and therapeutics, *Stem Cells Dev.* 13 (4) (2004) 436–448.
- [9] G.E. Friedlaender, et al., Osteogenic protein-1 (bone morphogenetic protein-7) in the treatment of tibial nonunions. *J Bone Joint Sur Am.* volume 2001;83-A Suppl 1 (Pt 2):S151–158.
- [10] K. Hu, B.R. Olsen, The roles of vascular endothelial growth factor in bone repair and regeneration, *Bone* 91 (2016) 30–38.
- [11] M. Wu, G. Chen, Y.P. Li, TGF-beta and BMP signaling in osteoblast, skeletal development, and bone formation, homeostasis and disease, *Bone Res.* 4 (2016) 16009.
- [12] T.J. Myers, et al., BMP2 regulation of CXCL12 cellular, temporal, and spatial expression is essential during fracture repair, *J. Bone Miner. Res.* 30 (11) (2015) 2014–2027.
- [13] D. Grcevic, et al., *In vivo* fate mapping identifies mesenchymal progenitor cells, *Stem Cells* 30 (2) (2012) 187–196.
- [14] C. Colnot, Skeletal cell fate decisions within periosteum and bone marrow during bone regeneration, *J. Bone Miner. Res.* 24 (2) (2009) 274–282.
- [15] M. Shahnazari, et al., CXCL12/CXCR4 signaling in the osteoblast regulates the mesenchymal stem cell and osteoclast lineage populations, *FASEB J.* 27 (9) (2013) 3505–3513.

- [16] M.J. Christopher, et al., Suppression of CXCL12 production by bone marrow osteoblasts is a common and critical pathway for cytokine-induced mobilization, *Blood* 114 (7) (2009) 1331–1339.
- [17] Z. Li, et al., Effects of altered CXCL12/CXCR4 axis on BMP2/Smad/Runx2/Osterix axis and osteogenic gene expressions during osteogenic differentiation of MSCs, *Am. J. Transl. Res.* 9 (4) (2017) 1680–1693.
- [18] Y. Jung, et al., Regulation of SDF-1 (CXCL12) production by osteoblasts; a possible mechanism for stem cell homing, *Bone* 38 (4) (2006) 497–508.
- [19] T. Sugiyama, et al., Maintenance of the hematopoietic stem cell pool by CXCL12-CXCR4 chemokine signaling in bone marrow stromal cell niches, *Immunity* 25 (6) (2006) 977–988.
- [20] V. Devescovi, E. Leonardi, G. Ciapetti, E. Cenni, Growth factors in bone repair, *Chir. Organi Mov.* 92 (3) (2008) 161–168.
- [21] R. Dimitriou, E. Jones, D. McGonagle, P.V. Giannoudis, Bone regeneration: current concepts and future directions, *BMC Med.* 9 (2011) 66.
- [22] R. Dimitriou, E. Tsiroidis, P.V. Giannoudis, Current concepts of molecular aspects of bone healing, *Injury* 36 (12) (2005) 1392–1404.
- [23] T.A. Einhorn, The cell and molecular biology of fracture healing, *Clin. Orthop. Relat. Res.* (355 Suppl) (1998) S7–S21.
- [24] E. Tsiroidis, N. Upadhyay, P. Giannoudis, Molecular aspects of fracture healing: which are the important molecules? *Injury* 38 (Suppl 1) (2007) S11–S25.
- [25] J.L. Crane, et al., IGF-1 signaling is essential for differentiation of mesenchymal stem cells for peak bone mass, *Bone Res.* 1 (2) (2013) 186–194.
- [26] G. Schmidmaier, et al., Long-term effects of local growth factor (IGF-I and TGF-beta 1) treated on fracture healing. A safety study for using growth factors, *J. Orthop. Res.* 22 (3) (2004) 514–519.
- [27] M.H. Sheng, K.H. Lau, D.J. Baylink, Role of osteocyte-derived insulin-like growth factor I in developmental growth, modeling, remodeling, and regeneration of the bone, *J. Bone Metabol.* 21 (1) (2014) 41–54.
- [28] S. Weiss, et al., Systemic response of the GH/IGF-I axis in timely versus delayed fracture healing, *Growth Hormon. IGF Res.* 18 (3) (2008) 205–212.
- [29] G. Zhao, et al., Targeted overexpression of insulin-like growth factor I to osteoblasts of transgenic mice: increased trabecular bone volume without increased osteoblast proliferation, *Endocrinology* 141 (7) (2000) 2674–2682.
- [30] S. Yakar, M.L. Adamo, Insulin-like growth factor 1 physiology: lessons from mouse models, *Endocrinol. Metabol. Clin. N.Am.* 41 (2) (2012) 231–247.
- [31] S. Weiss, et al., Systemic response of the GH/IGF-I axis in timely versus delayed fracture healing, *Growth Hormon. IGF Res.* 18 (3) (2008) 205–212.
- [32] C. Fischer, et al., Quantification of TGF- $\beta$ 1, PDGF and IGF-1 cytokine expression after fracture treatment vs. non-union therapy via masquelet, *Injury* 47 (2) (2016) 342–349.
- [33] A. Bernstein, H.O. Mayr, R. Hube, Can bone healing in distraction osteogenesis be accelerated by local application of IGF-1 and TGF-beta1? *J. Biomed. Mater. Res. B Appl. Biomater.* 92 (2010) 215–225.
- [34] G. Schmidmaier, et al., Improvement of fracture healing by systemic administration of growth hormone and local application of insulin-like growth factor-1 and transforming growth factor-beta1, *Bone* 31 (1) (2002) 165–172.
- [35] F. Westhauser, et al., Reaming in treatment of non-unions in long bones: cytokine expression course as a tool for evaluation of non-union therapy, *Arch. Orthop. Trauma Surg.* 135 (8) (2015) 1107–1116.
- [36] C.G. Tahimic, Y. Wang, D.D. Bikle, Anabolic effects of IGF-1 signaling on the skeleton, *Front. Endocrinol.* 4 (2013) 6.
- [37] K.W. Lau, et al., Conditional deletion of IGF-1 in osteocytes unexpectedly accelerates bony union of the fracture gap in mice, *Bone* 92 (2016) 18–28.
- [38] T. Wang, et al., Osteoblast-specific loss of IGF1R signaling results in impaired endochondral bone formation during fracture healing, *J. Bone Miner. Res.* 30 (9) (2015) 1572–1584.
- [39] Y. Wang, et al., IGF-1R signaling in chondrocytes modulates growth plate development by interacting with the PTHrP/Ihh pathway, *J. Bone Miner. Res.* 26 (7) (2011) 1437–1446.
- [40] Y. Wang, et al., IGF-1 signaling in osterix-expressing cells regulates secondary ossification center formation, growth plate maturation, and metaphyseal formation during postnatal bone development, *J. Bone Miner. Res.* 30 (12) (2015) 2239–2248.
- [41] Y. Wang, et al., Role of IGF-1 signaling in regulating osteoclastogenesis, *J. Bone Miner. Res.* 21 (9) (2006) 1350–1358.
- [42] K. Fulzele, et al., Disruption of the insulin-like growth factor type 1 receptor in osteoblasts enhances insulin signaling and action, *J. Biol. Chem.* 282 (35) (2007) 25649–25658.
- [43] J.L. Liu, S. Yakar, D. LeRoith, Conditional knockout of mouse insulin-like growth factor-1 gene using the Cre/loxP system, *Proc. Soc. Exp. Biol. Med.* 223 (4) (2000) 344–351.
- [44] K.E. Govoni, et al., Conditional deletion of insulin-like growth factor-I in collagen type 1alpha2-expressing cells results in postnatal lethality and a dramatic reduction in bone accretion, *Endocrinology* 148 (12) (2007) 5706–5715.
- [45] J. Jiang, et al., Transgenic mice with osteoblast-targeted insulin-like growth factor-I show increased bone remodeling, *Bone* 39 (3) (2006) 494–504.
- [46] L. Xian, et al., Matrix IGF-1 maintains bone mass by activation of mTOR in mesenchymal stem cells, *Nat. Med.* 18 (7) (2012) 1095–1101.
- [47] E. Antonova, T.K. Le, R. Burge, J. Mershon, Tibia shaft fractures: costly burden of nonunions, *BMC Musculoskelet. Disord.* 14 (2013) 42.
- [48] C. Britton, M.C. Poznansky, P. Reeves, Polyfunctionality of the CXCR4/CXCL12 axis in health and disease: implications for therapeutic interventions in cancer and immune-mediated diseases, *FASEB J.* 35 (4) (2021), e21260.
- [49] Y. Doring, L. Pawig, C. Weber, H. Noels, The CXCL12/CXCR4 chemokine ligand/receptor axis in cardiovascular disease, *Front. Physiol.* 5 (2014) 212.
- [50] B. Haribabu, et al., Regulation of human chemokine receptors CXCR4. Role of phosphorylation in desensitization and internalization, *J. Biol. Chem.* 272 (45) (1997) 28726–28731.
- [51] M.J. Orsini, et al., Trafficking of the HIV coreceptor CXCR4. Role of arrestins and identification of residues in the c-terminal tail that mediate receptor internalization, *J. Biol. Chem.* 274 (43) (1999) 31076–31086.
- [52] A. Hiltunen, E. Vuorio, H.T. Aro, A standardized experimental fracture in the mouse tibia, *J. Orthop. Res.* 11 (2) (1993) 305–312.
- [53] A. Esposito, et al., Role of Prx1-expressing skeletal cells and Prx1-expression in fracture repair, *Bone* 139 (2020), 115521.
- [54] F. Granero-Molto, et al., Mesenchymal stem cells expressing insulin-like growth factor-I (MSCIGF) promote fracture healing and restore new bone formation in Irs1 knockout mice: analyses of MSCIGF autocrine and paracrine regenerative effects, *Stem Cells* 29 (10) (2011) 1537–1548.
- [55] N. Ogata, et al., Insulin receptor substrate-1 in osteoblast is indispensable for maintaining bone turnover, *J. Clin. Invest.* 105 (7) (2000) 935–943.
- [56] T. Shimoaka, et al., Impairment of bone healing by insulin receptor substrate-1 deficiency, *J. Biol. Chem.* 279 (15) (2004) 15314–15322.
- [57] S. Yakar, H.W. Courtland, D. Clemmons, IGF-1 and bone: new discoveries from mouse models, *J. Bone Miner. Res.* 25 (12) (2010) 2543–2552.
- [58] L. Powell-Braxton, et al., Inactivation of the IGF-I gene in mice results in perinatal lethality, *Ann. N. Y. Acad. Sci.* 692 (1993) 300–301.
- [59] J. He, C.J. Rosen, D.J. Adams, B.E. Kream, Postnatal growth and bone mass in mice with IGF-1 haploinsufficiency, *Bone* 38 (6) (2006) 826–835.
- [60] J.P. Liu, et al., Mice carrying null mutations of the genes encoding insulin-like growth factor I (Igf-1) and type I IGF receptor (Igf1r), *Cell* 75 (1) (1993) 59–72.
- [61] L. Vandenput, K. Sjögren, J. Svensson, C. Ohlsson, The role of IGF-1 for fracture risk in men, *Front. Endocrinol.* 3 (2012) 51.
- [62] M. D'Apuzzo, et al., The chemokine SDF-1, stromal cell-derived factor 1, attracts early stage B cell precursors via the chemokine receptor CXCR4, *Eur. J. Immunol.* 27 (7) (1997) 1788–1793.
- [63] M. Shirozu, et al., Structure and chromosomal localization of the human stromal cell-derived factor 1 (SDF1) gene, *Genomics* 28 (3) (1995) 495–500.
- [64] L. Yu, et al., Identification and expression of novel isoforms of human stromal cell-derived factor 1, *Gene* 374 (2006) 174–179.
- [65] A. Aiuti, et al., Expression of CXCR4, the receptor for stromal cell-derived factor-1 on fetal and adult human lympho-hematopoietic progenitors, *Eur. J. Immunol.* 29 (6) (1999) 1823–1831.
- [66] Q. Ma, et al., Impaired B-lymphopoiesis, myelopoiesis, and derailed cerebellar neuron migration in CXCR4- and SDF-1-deficient mice, *Proc. Natl. Acad. Sci. U. S. A.* 95 (16) (1998) 9448–9453.
- [67] T. Nagasawa, et al., Defects of B-cell lymphopoiesis and bone-marrow myelopoiesis in mice lacking the CXC chemokine PBSF/SDF-1, *Nature* 382 (6592) (1996) 635–638.
- [68] Y.R. Zou, et al., Function of the chemokine receptor CXCR4 in haematopoiesis and in cerebellar development, *Nature* 393 (6685) (1998) 595–599.
- [69] A. Dar, O. Kollet, T. Lapidot, Mutual, reciprocal SDF-1/CXCR4 interactions between hematopoietic and bone marrow stromal cells regulate human stem cell migration and development in NOB/SCID chimeric mice, *Exp. Hematol.* 34 (8) (2006) 967–975.
- [70] T. Kitaori, et al., Stromal cell-derived factor 1/CXCR4 signaling is critical for the recruitment of mesenchymal stem cells to the fracture site during skeletal repair in a mouse model, *Arthritis Rheum.* 60 (3) (2009) 813–823.
- [71] S. Otsuru, et al., Circulating bone marrow-derived osteoblast progenitor cells are recruited to the bone-forming site by the CXCR4/stromal cell-derived factor-1 pathway, *Stem Cells* 26 (1) (2008) 223–234.
- [72] X. Yu, Y. Huang, P. Collin-Osdoby, P. Osdoby, Stromal cell-derived factor-1 (SDF-1) recruits osteoclast precursors by inducing chemotaxis, matrix metalloproteinase-9 (MMP-9) activity, and collagen transmigration, *J. Bone Miner. Res.* 18 (8) (2003) 1404–1418.
- [73] M. Baggiolini, Chemokines and leukocyte traffic, *Nature* 392 (6676) (1998) 565–568.
- [74] J.J. Lataillade, et al., Chemokine SDF-1 enhances circulating CD34(+) cell proliferation in synergy with cytokines: possible role in progenitor survival, *Blood* 95 (3) (2000) 756–768.
- [75] D.J. Ceradini, et al., Progenitor cell trafficking is regulated by hypoxic gradients through HIF-1 induction of SDF-1, *Nat. Med.* 10 (8) (2004) 858–864.
- [76] W.D. Hill, et al., SDF-1 (CXCL12) is upregulated in the ischemic penumbra following stroke: association with bone marrow cell homing to injury, *J. Neuropathol. Exp. Neurol.* 63 (1) (2004) 84–96.
- [77] M.Z. Ratajczak, et al., Expression of functional CXCR4 by muscle satellite cells and secretion of SDF-1 by muscle-derived fibroblasts is associated with the presence of both muscle progenitors in bone marrow and hematopoietic stem/progenitor cells in muscles, *Stem Cells* 21 (3) (2003) 363–371.
- [78] W. Zhu, et al., Conditional inactivation of the CXCR4 receptor in osteoprecursors reduces postnatal bone formation due to impaired osteoblast development, *J. Biol. Chem.* 286 (30) (2011) 26794–26805.
- [79] A. Caselli, et al., IGF-1-mediated osteoblastic niche expansion enhances long-term hematopoietic stem cell engraftment after murine bone marrow transplantation, *Stem Cells* 31 (10) (2013) 2193–2204.
- [80] Y.S. Tzeng, et al., Imbalanced osteogenesis and adipogenesis in mice deficient in the chemokine Cxcl12/Sdf1 in the bone mesenchymal stem/progenitor cells, *J. Bone Miner. Res.* 33 (4) (2018) 679–690.
- [81] I. Pusic, J.F. DiPersio, Update on clinical experience with AMD3100, an SDF-1/CXCL12-CXCR4 inhibitor, in mobilization of hematopoietic stem and progenitor cells, *Curr. Opin. Hematol.* 17 (4) (2010) 319–326.

- [82] P. Dietrich, et al., Conditional mutagenesis in mice with heat shock promoter-driven cre transgenes, *Mamm. Genome* 11 (3) (2000) 196–205.
- [83] M. Logan, et al., Expression of Cre recombinase in the developing mouse limb bud driven by a Prxl enhancer, *Genesis* 33 (2) (2002) 77–80.
- [84] A. Kawanami, T. Matsushita, Y.Y. Chan, S. Murakami, Mice expressing GFP and CreER in osteochondro progenitor cells in the periosteum, *Biochem. Biophys. Res. Commun.* 386 (3) (2009) 477–482.
- [85] E. Araki, et al., Alternative pathway of insulin signalling in mice with targeted disruption of the IRS-1 gene, *Nature* 372 (6502) (1994) 186–190.
- [86] F. Granero-Molto, et al., Regenerative effects of transplanted mesenchymal stem cells in fracture healing, *Stem Cells* 27 (8) (2009) 1887–1898.
- [87] M.L. Bouxsein, et al., Guidelines for assessment of bone microstructure in rodents using micro-computed tomography, *J. Bone Miner. Res.* 25 (7) (2010) 1468–1486.
- [88] J.D. Temple, T. Li, T.J. Myers, A. Spagnoli, High-resolution micro-computed tomography of articular cartilage and subchondral bone changes in mouse models of osteoarthritis, *OARSI Annual Meeting* (2013).
- [89] D.P. Mortlock, L.C. Post, J.W. Innis, The molecular basis of hypodactyly (Hd): a deletion in *hoxa 13* leads to arrest of digital arch formation, *Nat. Genet.* 13 (3) (1996) 284–289.
- [90] A.M. Parfitt, Bone histomorphometry: proposed system for standardization of nomenclature, symbols, and units, *Calcif. Tissue Int.* 42 (5) (1988) 284–286.
- [91] A. Balduino, et al., Bone marrow subendosteal microenvironment harbours functionally distinct haemosupportive stromal cell populations, *Cell Tissue Res.* 319 (2) (2005) 255–266.
- [92] A. Balduino, et al., Molecular signature and in vivo behavior of bone marrow endosteal and subendosteal stromal cell populations and their relevance to hematopoiesis, *Exp. Cell Res.* 318 (19) (2012) 2427–2437.
- [93] M. Crisan, M. Corselli, W.C. Chen, B. Peault, Perivascular cells for regenerative medicine, *J. Cell Molecul. Med.* 16 (12) (2012) 2851–2860.
- [94] M. Loibl, et al., Direct cell-cell contact between mesenchymal stem cells and endothelial progenitor cells induces a pericyte-like phenotype in vitro, *Bio. Med. Res. Intern.* (2014).
- [95] S. Mendez-Ferrer, et al., Mesenchymal and haematopoietic stem cells form a unique bone marrow niche, *Nature* 466 (7308) (2010) 829–834.
- [96] A. Tokunaga, et al., PDGF receptor beta is a potent regulator of mesenchymal stromal cell function, *J. Bone Min. Res.* 23 (9) (2008) 1519–1528.